

# EXTREME RADIO FLARES AND ASSOCIATED X-RAY VARIABILITY FROM YOUNG STELLAR OBJECTS IN THE ORION NEBULA CLUSTER

JAN FORBRICH,<sup>1,2</sup> MARK J. REID,<sup>2</sup> KARL M. MENTEN,<sup>3</sup> VICTOR M. RIVILLA,<sup>4</sup> SCOTT J. WOLK,<sup>2</sup>  
URVASHI RAU,<sup>5</sup> AND CLAIRE J. CHANDLER<sup>5</sup>

<sup>1</sup>*Centre for Astrophysics Research, School of Physics, Astronomy and Mathematics, University of Hertfordshire, College Lane, Hatfield AL10 9AB, UK*

<sup>2</sup>*Harvard-Smithsonian Center for Astrophysics, 60 Garden St, Cambridge MA 02138, USA*

<sup>3</sup>*Max-Planck-Institut für Radioastronomie, Auf dem Hügel 69, 53121 Bonn, Germany*

<sup>4</sup>*Osservatorio Astrofisico di Arcetri, Largo Enrico Fermi 5, 50125, Firenze, Italy*

<sup>5</sup>*National Radio Astronomy Observatory, P.O. Box O, Socorro, NM 87801, USA*

## ABSTRACT

Young stellar objects are known to exhibit strong radio variability on timescales of weeks to months, and a few reports have documented extreme radio flares, with at least an order of magnitude change in flux density on timescales of hours to days. However, there have been few constraints on the occurrence rate of such radio flares or on the correlation with pre-main sequence X-ray flares, although such correlations are known for the Sun and nearby active stars. Here we report simultaneous deep VLA radio and *Chandra* X-ray observations of the Orion Nebula Cluster, targeting hundreds of sources to look for the occurrence rate of extreme radio variability and potential correlation with the most extreme X-ray variability. We identify 13 radio sources with extreme radio variability, with some showing an order of magnitude change in flux density in less than 30 minutes. All of these sources show X-ray emission and variability, but only on timescales <1h do we find clear correlations with extreme radio flaring. Strong X-ray variability does not predict the extreme radio sources and vice versa. Radio flares thus provide us with a new perspective on high-energy processes in YSOs and the irradiation of their protoplanetary disks. Finally, our results highlight implications for interferometric imaging of sources violating the constant-sky assumption.

*Keywords:* radio continuum: stars, X-rays: stars, stars: coronae, stars: formation, stars: variables: T Tauri, Herbig Ae/Be

## 1. INTRODUCTION

Only a few examples of extreme radio flaring from young stellar objects (YSOs) – defined as flux density changing by more than an order of magnitude in less than a few hours – have been reported (e.g., [Bower et al. 2003](#); [Forbrich et al. 2008](#)). Other reported YSO radio variability is either less pronounced or becoming apparent on longer timescales of weeks to months (e.g., [Felli et al. 1993](#); [Zapata et al. 2004](#); [Rivilla et al. 2015](#)). However, the true occurrence rate is not known due to sensitivity limitations on short timescales. The spectral characteristics of such events are also poorly explored and, thus, it has been difficult to ascertain the relevant emission processes. Nonthermal radio emission at centimeter wavelengths in this context is usually interpreted as gyrosynchrotron radiation, created by mildly relativistic electrons gyrating in magnetic fields. The millimeter wavelength range provides access to synchrotron radiation from relativistic electron populations (e.g., [Güdel 2002](#)). While both X-ray and nonthermal radio emission in YSOs is thought to be produced in coronal-type activity (e.g., [Feigelson & Montmerle 1999](#)), X-ray flares are much better studied than radio flares (e.g., [Wolk et al. 2005](#); [Getman et al. 2008a,b](#)), and one outstanding question is whether or not radio and X-ray flares are physically related.

An empirical relation between the time-averaged radio and X-ray luminosities, the Güdel-Benz (GB) relation ([Güdel & Benz 1993](#); [Benz & Güdel 1994](#)), has been established for a wide range of active stars. For the Sun one also observes correlated X-ray and radio variability, the Neupert effect ([Neupert 1968](#)), where one observes magnetic energy release, from particle acceleration and injection to energy transformation and heating. In this relation, seen in some but not all flares, the time-integrated radio emission, which traces the energy injection, is proportional to the thermal X-ray emis-

sion. This phenomenon has been observed for a nearby active star ([Güdel et al. 2002](#)) and for one YSO ([Getman et al. 2011](#)).

In contrast to well studied X-ray flares from YSOs, only a handful of radio flares have been documented. [Bower et al. \(2003\)](#) reported an increase in flux density at a wavelength of 3.5 mm of a factor of 4–8 over hours for the evolved weak-line T Tauri star GMR A. Similar flares were reported from the weak-line T Tauri binary V773 Tau ([Massi et al. 2006](#)) and the classical T Tauri binary DQ Tau ([Salter et al. 2008](#)), most likely due to synchrotron radiation from inter-binary magnetic interactions. At a longer wavelength of 1.3 cm, [Forbrich et al. \(2008\)](#) reported an even stronger flare, with an increase in flux density of  $> 10$  in a few hours, toward the deeply embedded protostar termed the Orion Radio Burst Source (ORBS).

Both X-ray and radio flares provide clues related to the high-energy irradiation of the vicinities of YSOs and their protoplanetary disks. This irradiation may impact planet formation and planetary habitability. However, the connection between radio and X-ray emission remains unclear. This is partly due to observational limitations, since comparisons of flares on short timescales require simultaneous observations of phenomena that are not predictable and often weak. The radio flare of GMR A is one of only a few cases with simultaneous radio and X-ray coverage ([Bower et al. 2003](#)). Clearly, a larger sample of YSO extreme radio variability is needed to provide constraints on the association with X-ray flares.

We here continue the analysis of the first simultaneous radio and X-ray observations of YSOs following the sensitivity upgrade of the National Radio Astronomy Observatory’s Karl G. Jansky Very Large Array (VLA). The upgraded VLA is an interferometer with broad bandwidth and excellent instantaneous  $(u, v)$ -coverage to enable high-sensitivity studies of

YSOs. Using the VLA and *Chandra*, we have targeted the Orion Nebula Cluster (ONC), maximizing the chances of detecting YSO flares, since we can observe hundreds of YSOs in a single pointing. We have already published a catalog of 556 compact sources in the cluster, based on the entire concatenated radio dataset (Forbrich et al. 2016). The increased sensitivity of the VLA is now enabling access to shorter timescales than in previous such experiments, which have focused on time-averaged properties (Gagné et al. 2004; Forbrich et al. 2007; Osten & Wolk 2009; Forbrich et al. 2011; Forbrich & Wolk 2013).

In order to constrain the occurrence of extreme radio flares in these YSOs, akin to the event reported by Forbrich et al. (2008), we measured the radio light-curves of the all of these sources, looking for extreme changes in flux density, where “extreme” is defined as changes of more than an order of magnitude on timescales  $< 2$  days. Subsequently, we assessed the simultaneous X-ray variability of this sample of radio flares. The goal of this paper is to begin the exploration of YSOs in the radio–X-ray time domain by first identifying the most extreme variability.

## 2. OBSERVATIONS AND DATA ANALYSIS

While details of our Orion observations and the underlying source catalog can be found in Forbrich et al. (2016), we here briefly recount the main features of this experiment. We observed a single pointing position in the ONC for a total of 30 h over five days in the VLA’s highest-resolution A-configuration, using two spectral bands of 1 GHz width within the C-band (4–8 GHz) receivers, centered at 4.736 GHz and 7.336 GHz. During the first two epochs, the array was being re-configured to the A configuration from the BnA configuration. The VLA observations were accompanied by 24 h of nearly simultaneous *Chandra* observations. The observing log is listed in Ta-

**Table 1.** Observing log

Epoch	Observatory	Time range
1	VLA	2012-Sep-30 07:33 – 15:01
	<i>Chandra</i>	–
2	VLA	2012-Oct-02 07:25 – 14:53
	<i>Chandra</i>	2012-Oct-02 07:02 – 15:16
3	VLA	2012-Oct-03 13:20 – 16:19
	<i>Chandra</i>	2012-Oct-03 12:53 – 15:56
4	VLA	2012-Oct-04 10:49 – 16:00
	<i>Chandra</i>	2012-Oct-04 08:21 – 16:13
5	VLA	2012-Oct-05 08:28 – 16:11
	<i>Chandra</i>	2012-Oct-05 10:42 – 16:17

ble 1. In the following, all source numbers refer to the source catalog in (Forbrich et al. 2016), with the prefix [FRM2016].

We have sliced the entire dataset into short time intervals and imaged independently. Without precise constraints on the most relevant timescale, and given the trade-off between high time resolution and sensitivity, we produced three sets of images over timescales of 6 hours, 30 minutes, and 6 minutes. We here focus on imaging in Stokes-*I*. The latter two sets of images are limited somewhat by problems associated with varying  $(u, v)$ -coverage for some resolved sources, varying source strength during the integration period, and their distribution over a wide field comparable to the individual antenna primary beamwidth.

Imaging was done in the Common Astronomy Software Applications package (CASA, McMullin et al. 2007) as had been done for the concatenated dataset (Forbrich et al. 2016), including the same approximate correction for the primary beam attenuation. For the two

sets of maps with higher time resolution, with different synthesized beam shapes and sizes per time bin, we chose a smaller pixel size of  $0''.04$ , instead of  $0''.10$ . Since we left the image size at  $8192 \times 8192$  pixels (for computational reasons), this resulted in a field of view of  $5''.4 \times 5''.4$ , which excluded some sources in the outermost portion of the primary beam. However, the images still covered 507 of the 556 sources in our catalog. Additionally, prior to imaging, we time averaged 10 sec, in order to speed up the computations, at a modest cost of a few percent in flux density loss for sources near the edges of the maps (e.g., KM Ori [Forbrich et al. 2016](#)). Only a few of the mapped time intervals were discarded based on poor image quality (see below).

As for our original catalog, we fitted all sources using “jmfitt” of the Astronomical Image Processing System (AIPS<sup>1</sup>). We assumed a model of a single Gaussian component to determine the peak flux density, provided the peak was within a few pixels of the catalog position and had a signal-to-noise ratio greater than 4. Such fits work best for point sources, since otherwise the changing synthesized beam can interact with the complex source structure to introduce spurious variability. Many sources detected in the concatenated image were not detected with the lower sensitivity afforded by the higher time resolution. To assess the inter-epoch calibration, we selected the 223 sources detected at all five epochs. Removing the 10% most variable ones, left 201 sources. Averaging their peak flux densities yield identical values to within a few percent,  $0.520 \pm 0.015$  mJy/beam, indicating very good inter-epoch calibration.

This paper describes only the most extreme varying sources that comprise only 2–3% of radio sources. Many sources exhibit significant variability below our extreme threshold, but

they are beyond the scope of this paper. At low levels of variability, systematic effects like the impact of the changing  $(u, v)$  coverage on resolved sources and the wideband primary beam are difficult to quantify and remove.

### 2.1. X-ray observations

Our radio observations for epochs 2–5 had simultaneous X-ray observations by *Chandra* (see Table 1). The *Chandra* observations were reduced using `acis_extract` ([Broos et al. 2010](#)), and the catalog of the *Chandra* Orion Ultradeep Project (COUP) ([Getman et al. 2005b](#)) was used as an input catalog for point source extraction. The code `acis_extract` extracts information from multiple observing epochs, taking into account different spacecraft parameters and, in particular, differing point-spread functions at different epochs, and it combines this information into global metrics across all epochs. Of particular interest here are the extracted X-ray lightcurves and variations of median photon energy as a sensitive tracer of spectral changes. While the code also extracts spectra and concatenates these across observing epochs, our focus here is on these time series metrics.

## 3. RADIO ANALYSIS

A total of 13 sources showed extreme radio variability (greater than a factor of  $\Delta S=10$ ) on timescales of less than 2 days. Their positions are shown in Figure 1 and details are listed in Table 2, including i) the maximum variability factor, ii) the minimum timescale where variability by a factor of at least 10, and iii) the peak flux densities from the concatenated data, as derived by [Forbrich et al. \(2016\)](#). Radio lightcurves for these sources at all imaging timescales are shown in Figure 4.

In [Forbrich et al. \(2008\)](#) we used the BN object, a non-variable thermally emitting source [Forbrich et al. \(2016\)](#), to assess the magnitude of systematic effects affecting measured variabil-

<sup>1</sup> <http://www.aips.nrao.edu>

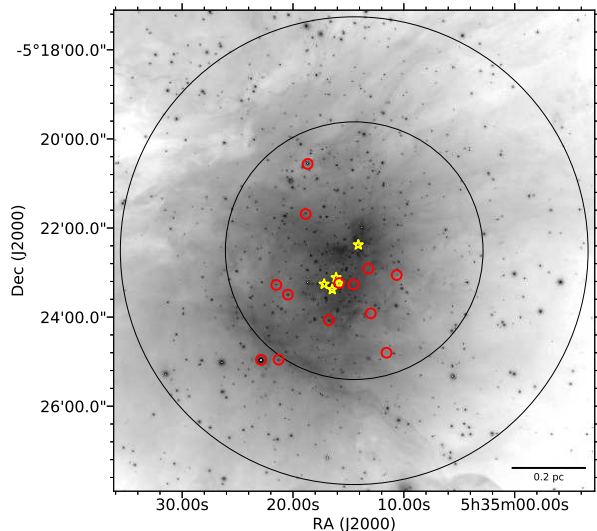


**Figure 1.** Distribution of the 13 radio sources showing extreme radio variability (by a factor  $> 10$ ), at any of the three time-scales discussed in the text, overlaid on the VISION- $K_S$  image from Meingast et al. (2016). For orientation, the locations of the Trapezium ( $\theta^1$  Ori A) and the BN object are marked with star symbols. The circles indicate the smallest (i.e., highest-frequency) and largest C-band HPBW primary beams, and the scale bar indicates the physical scale at a distance of 414 pc.

ity. This source is number 162 in our catalog; it is bright and marginally resolved, and it could show effects both due to the wideband primary beam and to changing  $(u, v)$ -coverage. In our time series data, the standard deviation of its peak flux density is  $< 11\%$ , and we conclude that systematics have not significantly affected our findings presented here.

### 3.1. Individual epochs

We find only 244 out of 556 previously catalogued sources are detected in all five epochs, partly due to the lower sensitivity compared to the concatenated data and partly due to variability. The rms noise levels range between 12 and 19  $\mu\text{Jy bm}^{-1}$  due to the different du-

rations of the individual epochs. Seven sources meet our criteria for extreme variability (see Table 2) at these imaging integration times. Two sources are outside of the primary beam half-power radius at the higher frequency band and, thus, are not included in the following discussion<sup>2</sup>. Source 515 displays the greatest change in flux density, a factor of 57. Some sources were detected in just one epoch, but strong enough to produce a detection in the concatenated dataset.

We note that the averages of the peak flux densities of the individual epochs do not always agree with the values from imaging with the concatenated dataset (Forbrich et al. 2016). This discrepancy is a result of strong variability during the imaging integration time, which can scatter power away from the source in a complicated manner. This finding is a warning that flux densities and spectral indices of strongly variable sources can be erroneous when the integration time is longer than the variability time scale.

### 3.2. 30 min intervals

At 30 min time resolution we made 57 images, with median rms noise of 34  $\mu\text{Jy bm}^{-1}$ . Owing to reduced sensitivity from short integrations, 76 (out of 507) sources were not detected in any image, and only 48 sources have  $> 3\sigma$  detections in all 30 min bins. All seven sources identified from individual epoch images are confirmed to be extreme variables in the 30-min images. In addition, five other sources (98, 110, 254, 469, and 495) now show extreme variability, with sources 110 and 469 displaying particularly extreme variations. In a few cases, the variability amplitude appears to decrease when compared to the by-epoch assessment, but only when flux density upper limits are involved, such that the resulting variability amplitudes are statistically

<sup>2</sup> Sources 358 and 459 are varying by factors of  $> 18$  and  $> 20$ , respectively, on a timescale of two days.



compatible with each other. A visualization of the selection process is shown in Figure 2.

### 3.3. 6 min intervals

Finally, we made 332 images from 6-min integrations. (At this sampling rate, nine integrations produced anomalous noise levels and were discarded.) Naturally, the median rms noise of  $56 \mu\text{Jy bm}^{-1}$  per image increased compared to the 30-min integrations, and 83 catalog sources were not detected in any 6-min image. Only source number 400 (GMR F) is detected in every single 6 min bin, but 70 sources have detections in at least half of the bins. Imaging artifacts due to poor  $(u, v)$ -coverage increase and produce occasional strong outliers in the lightcurves.

In total, we detect eight extreme variable sources with 6-min integrations. Only one of these (number 414) had not been found in the longer time integrations. This brings the total count of extreme variable sources to 13. For three sources (254, 319, 469), the amplitude of variability is greater than determined from the longer integrations, and more such cases may be hidden in cases where flux density upper limits are involved. The lightcurves of some sources show spectacular detail; sources 98, 469, and 515 show strong flares (Figure 4), with flux density changes by more than a factor of 10 over 0.4 to 0.7 h (see Table 2). Source 515 shows the strongest flare, with a peak shortly before the end of the observations. The remaining sources show irregular variability, and many remain undetected over entire multi-hour epochs at this timescale. A visualization of the selection process is shown in Figure 3.

### 3.4. Individual 90 sec scans

To study the bright flare of source 515 in the third epoch in more detail, we have imaged 60 individual 90 sec scans, and the light curve is shown in Figure 5. The flux densities are marginally higher than with a resolution of

6 min, and a turnover before the end of the observation now is visible more clearly than at a resolution of 6 minutes.

### 3.5. Occurrence rate of extreme radio variability

We now estimate the occurrence rates of extreme radio variability of Orion YSOs on different timescales. While our search has targeted all 507 sources catalogued in Forbrich et al. (2016) that lie within a more limited field of view, that full source count is not the best reference sample since, as we have discussed in that paper, several of the radio sources are likely non-stellar. Assuming that the most complete sample of YSOs in the inner ONC is the COUP X-ray sample (Getman et al. 2005a) and noting that all 13 radio flare sources identified here indeed have COUP X-ray counterparts, our reference sample thus consists of those 222 radio sources among the 507 studied here that have X-ray counterparts.

From the cumulative radio observing time of these sources of about  $222 \times 30 = 6,660$  hours, we find only three flares with a flux density change of more than a factor of 10 on timescales less than hour. Assuming a detectable flare duration of 2 h, we thus estimate that each of these sources displays on average such a flare only  $\approx 0.09 \pm 0.05\%$  of the time, assuming a Poisson error in the flare count of  $\pm\sqrt{3}$ . Thus, the mean time between such flares is  $2220 \pm 1280$  h, or  $8.0 \pm 4.6$  Msec, or roughly every three months. This is, of course, only a crude estimate, since it assumes a homogeneous underlying sample.

On time scales longer than  $\approx 1$  h, we have identified 13 sources with order-of-magnitude changes in flux density on timescales of several hours to days (although this number is uncertain because of unavoidable gaps in the observing schedule). Thus, extreme variability on these longer timescales seems to occur roughly once every three weeks. In the context of variability on longer timescales, we note finally that

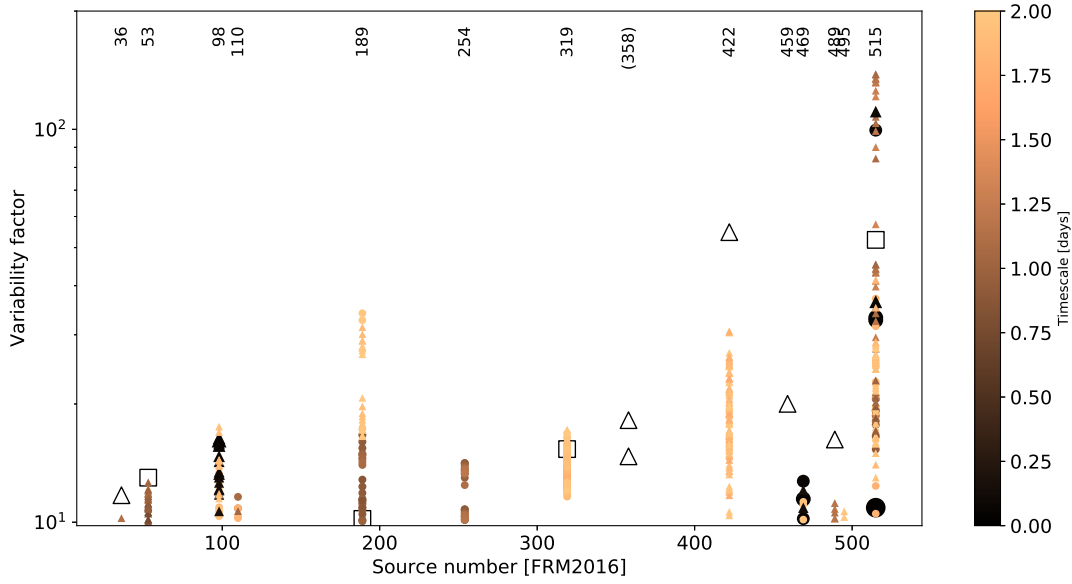


**Figure 2.** Selection of extremely variable sources at a resolution of 30 min. The variability factors  $> 10$  from all two-point comparisons are plotted, on a logarithmic scale and by source number. The color encodes the associated timescale for the respective point pair, which is also highlighted by symbol size. Triangles denote lower limits. Finally, the large open symbols show the selection for data from the individual epochs. Labels additionally designate the source numbers, with source 358 in brackets because no data at high time resolution is available.

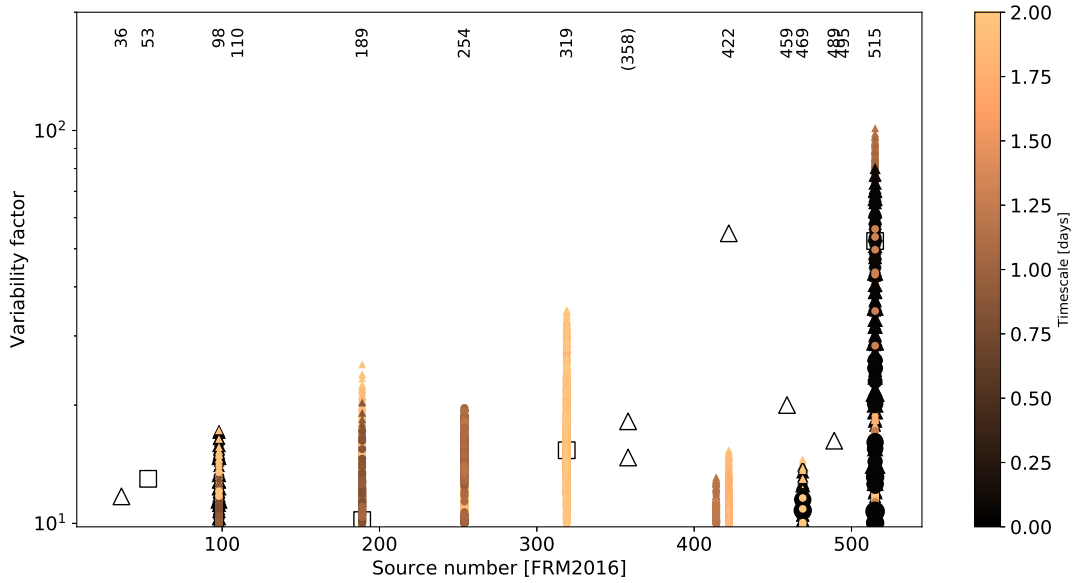


**Figure 3.** Selection of extremely variable sources at a resolution of 6 min; see Figure 2 for details.

of the 13 variable sources that we identify here, a total of nine sources have been detected in previous VLA observations (see Table 2), albeit with different sensitivity limits.

### 3.6. X-ray and infrared identification

Interestingly, the 13 sources of extreme radio variability that we identified all have X-ray counterparts in the deep *Chandra* observations reported by Getman et al. (2005b), and also in the simultaneous *Chandra* observations reported here. All but three of them (sources 98, 110, and 189) also have near-infrared counterparts in the VISION survey (Meingast et al. 2016). Based on their X-ray and near-infrared characteristics, all 13 sources have previously been identified as YSOs (Broos et al. 2013). Sources without near-infrared counterparts could be missed if they are deeply embedded or are projected on bright nebulosity. Eight of the sources have reported spectral types in the literature, ranging from O to M, even if it remains unclear, in the case of the most massive stars, whether the radio emission might instead come from an unresolved low-mass companion. Source 469 is a well-resolved M0+M3.5 binary<sup>3</sup> (Daemgen et al. 2012). The extreme variability originates on the M0 main component. The cross-identifications are summarized in Table 2.

## 4. SIMULTANEOUS X-RAY OBSERVATIONS

In the analysis of our simultaneous X-ray observations, our focus here is to determine if the extreme radio variability is associated with unusual X-ray variability, since general studies of X-ray flares of YSOs have appeared elsewhere. We analyzed our *Chandra* observations with the *acis\_extract* software package (Broos et al. 2010) in order to obtain X-ray lightcurves and time series of median photon en-

ergy for all sources that had already been studied by Getman et al. (2005b). Here we only discuss the X-ray lightcurves of the extreme variable radio sample.

The net X-ray counts for the present sample of 13 sources are listed in Table 2; they range from a few to more than 8000 counts. The brightest X-ray sources show some photon pile-up, where the count rate is high enough that two or more photons may have been counted as a single event, affecting a more detailed analysis. The *acis\_extract* program estimates that this could affect seven out of 13 sources, marked with asterisks in Table 2. The strongest pile-up effect is expected toward the brightest source 254, with an estimated count rate of 0.4 ct/frame. We have used the pile-up correction tool described in Broos et al. (2011), and we estimate a pile-up correction of  $\sim 45\%$  for this strong source. The pile-up correction, where applicable, thus ranges from  $\sim 10\%$  to  $\sim 45\%$ . This effect might alter the shape of extracted lightcurves and the assignment of photon energies, but not at a level that would be a concern for the analysis presented here.

To assess the X-ray variability in the sample, we follow the *acis\_extract* approach to analyze both a binned lightcurve and also a smoothed unbinned lightcurve, built using the photon arrival times and adaptive kernel smoothing (Broos et al. 2010). The latter is particularly useful to identify substructure that changes on timescales shorter than the bin size. The X-ray lightcurves for the extremely variable radio sources are shown in Figure 6, together with the simultaneous portions of the radio lightcurves. To match up the X-ray and radio data, we have converted the time axes of the radio lightcurves to the time axes of the X-ray lightcurves, in cumulative *Chandra* elapsed time (in kiloseconds).

While the focus of this paper is extreme radio variability, we have also quantified extreme X-ray variability in the four epochs of *Chandra*

<sup>3</sup> Both components are detected in our radio observations, if marginally in the case of the M3.5 star.



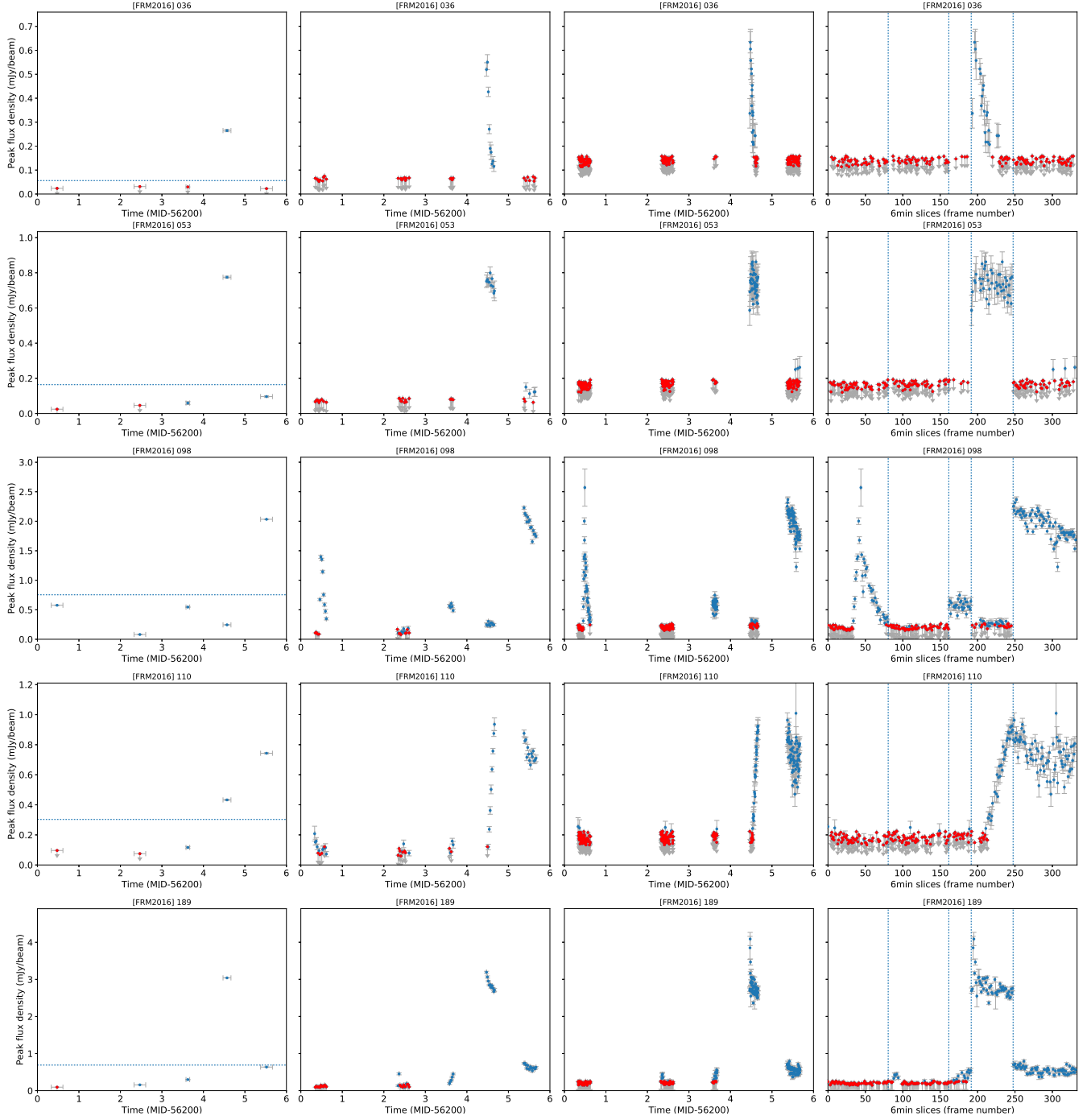


**Figure 4.** Radio lightcurve synopsis with peak flux densities corrected for the primary beam response. Detections are marked in blue, errors in grey, and upper limits in red. The left-hand panel compares the peak flux density from the concatenated data (dotted line) with the numbers from the individual epochs. The other three panels show the data at 30 min resolution and at 6 min resolution, the latter both with a time axis and sequential frames to highlight details.

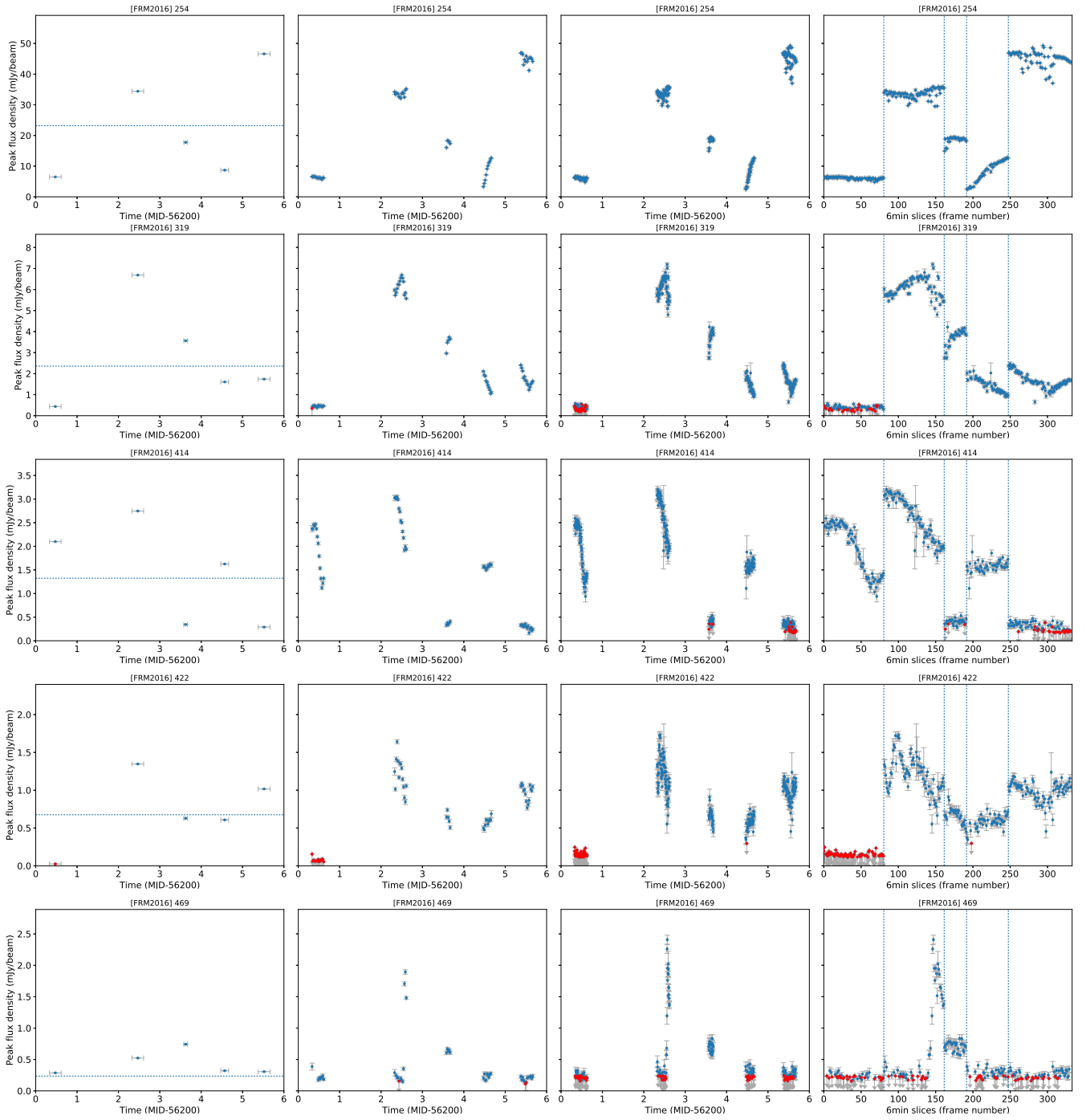
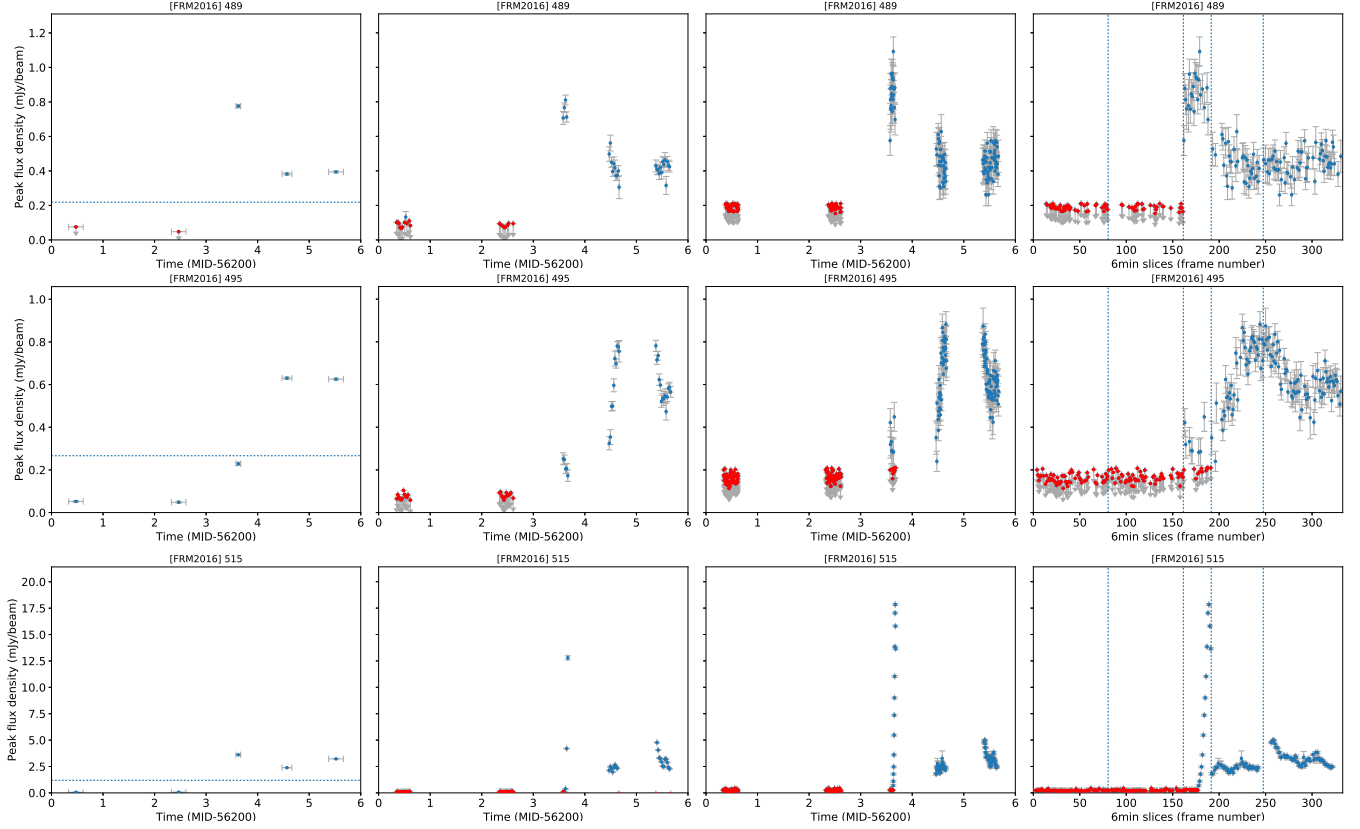


Figure 4 cntd.



**Figure 4** cntd.

data. This allows us to quantify to what degree extreme radio and X-ray variability are correlated. To quantify extreme X-ray variability, we use the “glvary” algorithm of the Chandra Interactive Analysis of Observations software package (CIAO, [Gregory & Loredo 1992](#); [Rots 2006](#)). This program uses the Gregory-Loredo variability test algorithm on the unbinned X-ray data, using multiple different time bins and looking for significant deviations. As a result, it computes a variability index (“varindex”) on a scale of 0 to 10, where 0 corresponds to a source that is definitely not variable and 6 for a source that is definitely variable. A varindex of 10 indicates extreme variability akin to a flare.

We determine the varindex for three different source samples on a per-epoch basis. For the first sample, we take all detected X-ray sources, but we discard those sources with distances from the VLA phase center that are larger than the outermost radio detection of 6°785, thereby

ensuring an approximate comparability of the radio and X-ray samples. This step discards 164 out of 1129 X-ray sources for a total sample size of 965 sources. The second sample consists of those X-ray sources that have radio counterparts in our observations, as listed in our catalog paper, resulting in a sample of 228 sources. The third sample consists of the 13 sources defined as extreme variable radio sources in the present paper.

After determining the varindex values for these samples at all four X-ray epochs, we pick the maximum varindex for each source to quantify variability within the epochs. A source with varindex=10 in any one epoch thus is listed with this varindex while a varindex of 0 means that it has been zero in all four epochs. The resulting distributions of the maximum varindex values per source for the three samples are shown in [Figure 7](#).

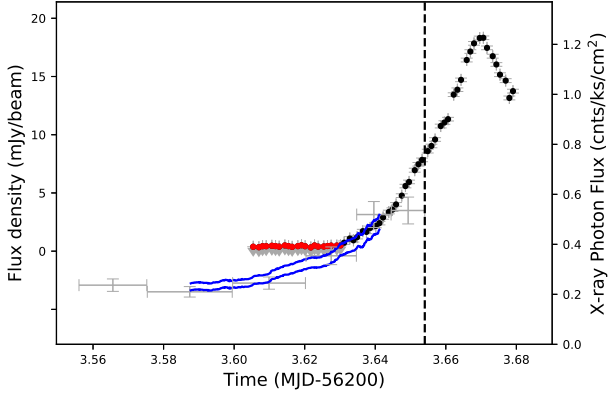


**Figure 5.** Radio lightcurve of source 515, at a time resolution of 90 sec, showing only the flare in epoch 3, with data points in black and upper limits in red (left axis). Shown additionally, in blue, are the confidence intervals of the adaptively smoothed X-ray light curve from *acis\_extract* (right axis; same as in Figure 4), and a binned version of the same lightcurve with 100 counts per bin (90 in the first bin). To show that both lightcurves likely trace the same event, both scales have been linearly shifted with respect to each other so that the lightcurves match up. The vertical dashed line indicates the end of the *Chandra* observation.

The varindex distributions are spread across all possible values from 0 to 10. Most sources have little or no variability, but a total of 18 sources do show the highest possible varindex=10. Interestingly, only five of these sources have radio counterparts in our sample, and only two of these are in the sample of extremely variable radio sources.

The extreme variable radio sources do not seem to have unique X-ray varindex properties. Instead, they generally fall into two very different groups. Most of them, 7 out of 13 sources, have varindex=0 to 2, while 4 sources have varindex=9 to 10, with just two sources in-between (at varindex=5 and 6). It is remarkable, though, that the three radio sources that vary on hour timescales (sources 36, 469, 515) have a varindex of either 9 or 10.

## 5. SIMULTANEOUS RADIO AND X-RAY VARIABILITY

With the extreme radio variability and the corresponding X-ray variability presented, we now assess the correlation between them. The first step is to determine whether extreme radio variability within a single observing epoch coincides with X-ray flaring. While there could well be a lag between the two types of variability, we lose sensitivity to this connection once the lag is longer than the duration of the observing epochs, since a related but delayed flare could fall into one of the gaps in-between our observing epochs.

We start with the three sources (98, 469, and 515) with extreme radio variability on less than hour timescales. The radio flare in source 98 occurs in the first epoch, which unfortunately does not have *Chandra* coverage. However, the radio flares of sources 469 and 515 both coincide with simultaneous X-ray variability, although this only becomes apparent in the adaptively smoothed lightcurves, as binning on timescales longer than a flare can average away the detection. The X-ray flares are not very strong, and statistically the events coincide; there is no evidence for a significant offset in time.

Moving to other sources which exhibited extreme radio flaring on longer timescales, source 36 also displayed near simultaneous radio and X-ray flares. Its X-ray flare is best detected in the adaptively binned lightcurve and its radio variability stays just below an order of magnitude change in its flux density within a single epoch, but it reaches this threshold when considering neighboring epochs. Interestingly, source 110 displays a radio flare with a steep slope, there is no detected X-ray flare. However, this source is generally a very weak X-ray source, and the non-detection may thus be due to insufficient sensitivity.

Overall, the results shown in Figure 6 qualitatively show varying levels of radio-X-ray cor-

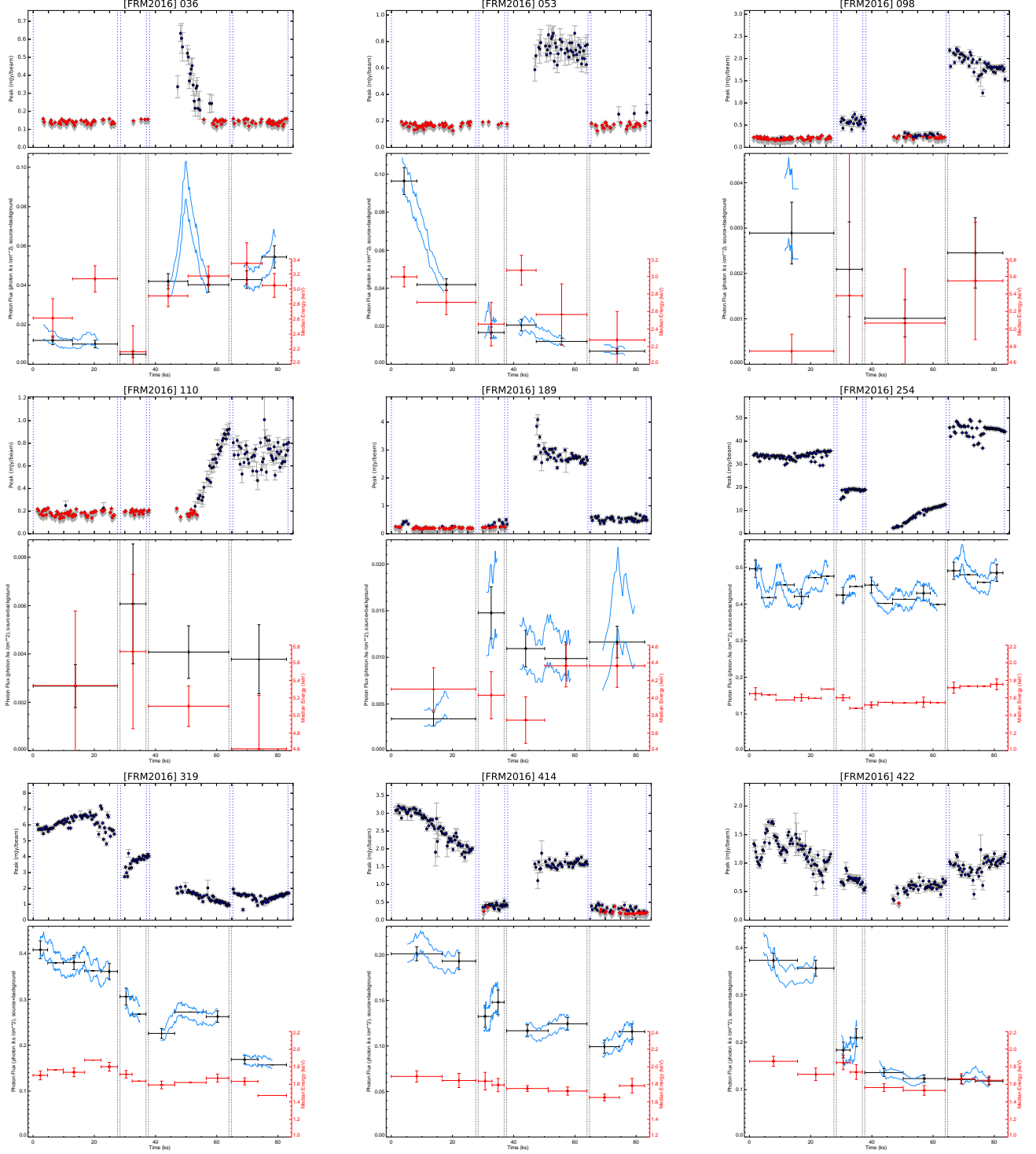


**Figure 6.** Simultaneous radio and X-ray lightcurves. The upper panel for each source shows the same radio data, at 6 min time resolution, that is also shown in Figure 4, but only if the data coincide with X-ray observations. The time axis of the radio lightcurves has been converted to match the cumulative *Chandra* elapsed time in ksec. The lower panel shows both a binned X-ray lightcurve (black crosses) and a binned median photon energy curve (red crosses). Additionally, it shows the upper and lower confidence intervals of the adaptively smoothed photon counts (blue), see [Broos et al. \(2010\)](#).



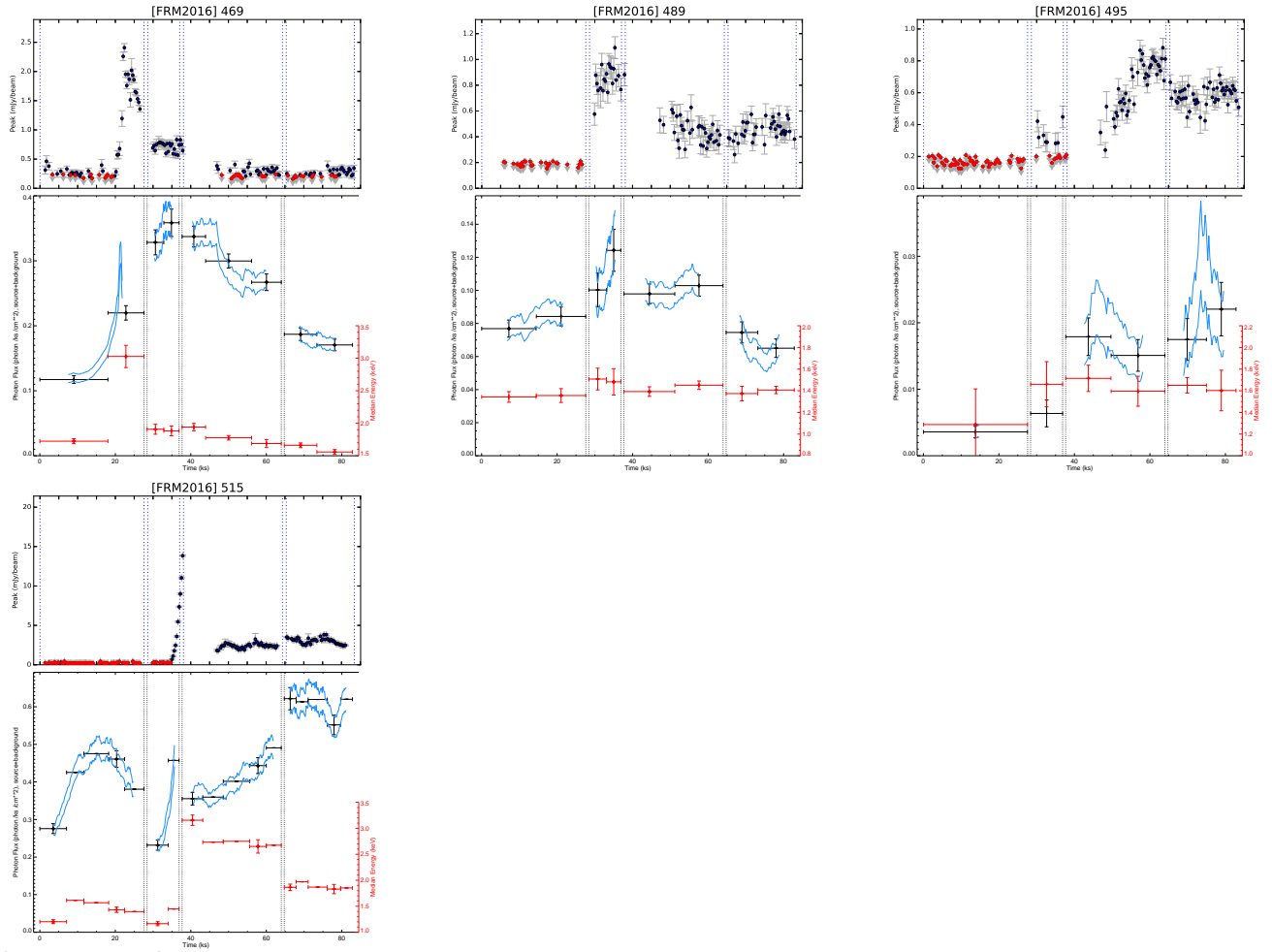
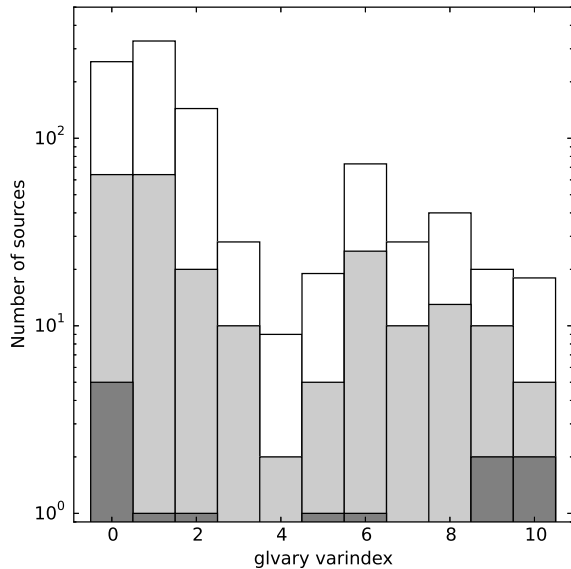


Figure 6 cntd.



**Figure 7.** X-ray variability, as quantified with the glvray varindex (see text), for the full sample of X-ray sources within the radio field of view (white bins), the subsample with radio counterparts (light grey bins), and the subsample of the 13 extremely variable radio sources identified in this paper (dark grey bins). Note the logarithmic y axis.

relation across multiple epochs. In many cases, there is no correlation between overall flux levels or trends between epochs. In some cases, this is influenced by insufficient sensitivity in either band, but even bright X-ray sources show phenomena as diverse as no correlation whatsoever (source 254) or significant correlation (source 319).

When comparing the radio and X-ray lightcurves, it thus emerges that extreme radio variability is clearly correlated with X-ray variability *only on very short timescales*. However, on timescales of days, we find complexity in the lightcurves, but do not see clear trends. associating X-ray and radio variability. Because of the unavoidable gaps in coverage for the ground-based radio observations, it is impossible to know whether or not an apparent overall correlation as seen

toward source 319 traces a common event or is a coincidence of unrelated activity.

### 5.1. Outlook

Our first results demonstrate how the upgraded VLA, with greatly increased sensitivity, is providing us with a new perspective on high-energy processes in YSOs, by allowing us to systematically study YSO radio emission on timescales of minutes. This is complementary to the X-ray view, which by now is much better documented. Understanding connections between emissions in these wavebands may be particularly important for a full assessment of the high-energy irradiation of protoplanetary disks.

Based on this first estimate of extreme centimeter-wavelength variability, it will now also be interesting to systematically probe extreme variability involving even higher energy electrons in the millimeter-wavelength range, using the Atacama Large Millimeter Array (ALMA), where synchrotron may dominate over gyro-synchrotron emission (e.g., [Massi et al. 2006](#)).

A general assessment of YSO radio variability will be presented after complex corrections for time- and position-dependent effects of the wideband primary beam, impacting variability, polarization, and spectral indices ([Bhatnagar et al. 2013](#)). Finally, our results highlight the inadequacy of a constant-sky assumption in interferometric imaging in this scenario. For the extreme radio variability reported here, the single integrated flux density and spectral index, as for example reported in our deep catalog, is of questionable value. It will soon be possible, however, to incorporate a model of a variable sky in the imaging process (e.g., [Rau 2012](#)). The upgrade to wideband continuum receivers thus has resulted in fantastic new opportunities while also posing new calibration and imaging challenges, mostly involving the abandonment of the assumptions of monochromatic imaging of a constant sky.

## 6. SUMMARY

This study presents a first systematic assessment of extreme radio variability in YSOs and the connection with X-ray variability from simultaneous observations. Our main results can be summarized as follows:

- Thirteen of 507 radio sources show extreme variability, defined as a factor of  $> 10$  and on timescales shorter than two days. All of these extremely variable sources are X-ray sources, so 13 out of 222 radio sources with X-ray counterparts fall into this category, or about 6%. The most extreme variability on timescales of less than two days is by a factor of  $> 138$ .
- Three sources show such extreme radio variability on timescales of just 0.4 to 0.7 hours. We estimate an average occurrence rate of one such extreme short-timescale flare per star in about three months.
- For two of the short-timescale radio events (in sources 469 and 515) we had simultaneous X-ray observations, and these radio flares were accompanied by quasi-simultaneous, equally short-duration, X-ray flares. A third source (36) shows similar behavior, even if it stays short of a variability factor of 10 at the highest time resolution. Beyond these short-duration radio flares, the correlation of radio and X-ray variability is less clear, and we find cases both of apparent correlation as well as seemingly uncorrelated behaviour.
- The sample of variable radio sources contains stars with spectral types ranging from O to M stars, indicating that extreme radio variability occurs across the stellar mass range, unless the emission

from higher mass stars comes from unresolved low-mass companions.

- In X-rays, we find that only five out of 18 of the most variable X-ray sources ( $\text{varindex}=10$ ) in the common field of view have radio counterparts, and only two of these are in the sample of extremely variable radio sources. However, five of the 13 extremely variable radio sources show no X-ray variability ( $\text{varindex}=0$ ), indicating a complex time domain connection, or lack thereof, between YSO radio and X-ray emission.

Support for this work was provided by the National Aeronautics and Space Administration through Chandra Award Number GO2-13019X issued by the Chandra X-ray Observatory Center, which is operated by the Smithsonian Astrophysical Observatory for and on behalf of the National Aeronautics Space Administration under contract NAS8-03060. The National Radio Astronomy Observatory is a facility of the National Science Foundation operated under cooperative agreement by Associated Universities, Inc. JF would like to thank Pat Broos, for insightful help with and advice on `acis_extract`, and acknowledge [Liebovitch \(1974\)](#) as a continuing source of inspiration for time domain science. V.M.R. is funded by the Italian Ministero dell'Istruzione, Università e Ricerca through the grant Progetti Premiali 2012 - iALMA.

*Facilities:* VLA, CXO

*Software:* CASA, [McMullin et al. 2007](#), AIPS, <http://www.aips.nrao.edu>, CIAO, [Gregory & Loredo 1992](#); [Rots 2006](#), `acis_extract`, [Broos et al. 2010](#)

## REFERENCES

- Benz, A. O., & Güdel, M. 1994, *A&A*, 285, 621
- Bhatnagar, S., Rau, U., & Golap, K. 2013, *ApJ*, 770, 91

- Bower, G. C., Plambeck, R. L., Bolatto, A., et al. 2003, *ApJ*, 598, 1140
- Broos, P. S., Townsley, L. K., Feigelson, E. D., et al. 2010, *ApJ*, 714, 1582
- . 2011, *ApJS*, 194, 2
- Broos, P. S., Getman, K. V., Povich, M. S., et al. 2013, *ApJS*, 209, 32
- Daemgen, S., Correia, S., & Petr-Gotzens, M. G. 2012, *A&A*, 540, A46
- Feigelson, E. D., & Montmerle, T. 1999, *ARA&A*, 37, 363
- Felli, M., Taylor, G. B., Catarzi, M., Churchwell, E., & Kurtz, S. 1993, *A&AS*, 101, 127
- Forbrich, J., Menten, K. M., & Reid, M. J. 2008, *A&A*, 477, 267
- Forbrich, J., Osten, R. A., & Wolk, S. J. 2011, *ApJ*, 736, 25
- Forbrich, J., & Wolk, S. J. 2013, *A&A*, 551, A56
- Forbrich, J., Preibisch, T., Menten, K. M., et al. 2007, *A&A*, 464, 1003
- Forbrich, J., Rivilla, V. M., Menten, K. M., et al. 2016, *ApJ*, 822, 93
- Gagné, M., Skinner, S. L., & Daniel, K. J. 2004, *ApJ*, 613, 393
- Getman, K. V., Broos, P. S., Salter, D. M., Garmire, G. P., & Hogerheijde, M. R. 2011, *ApJ*, 730, 6
- Getman, K. V., Feigelson, E. D., Broos, P. S., Micela, G., & Garmire, G. P. 2008a, *ApJ*, 688, 418
- Getman, K. V., Feigelson, E. D., Grosso, N., et al. 2005a, *ApJS*, 160, 353
- Getman, K. V., Feigelson, E. D., Micela, G., et al. 2008b, *ApJ*, 688, 437
- Getman, K. V., Flaccomio, E., Broos, P. S., et al. 2005b, *ApJS*, 160, 319
- Gregory, P. C., & Lored, T. J. 1992, *ApJ*, 398, 146
- Güdel, M. 2002, *ARA&A*, 40, 217
- Güdel, M., Audard, M., Smith, K. W., et al. 2002, *ApJ*, 577, 371
- Güdel, M., & Benz, A. O. 1993, *ApJL*, 405, L63
- Hillenbrand, L. A., Hoffer, A. S., & Herczeg, G. J. 2013, *AJ*, 146, 85
- Kounkel, M., Hartmann, L., Loinard, L., et al. 2014, *ApJ*, 790, 49
- Liebovitch, L. S. 1974, *QJRAS*, 15, 141
- Massi, M., Forbrich, J., Menten, K. M., et al. 2006, *A&A*, 453, 959
- McMullin, J. P., Waters, B., Schiebel, D., Young, W., & Golap, K. 2007, in *Astronomical Society of the Pacific Conference Series*, Vol. 376, *Astronomical Data Analysis Software and Systems XVI*, ed. R. A. Shaw, F. Hill, & D. J. Bell, 127
- Meingast, S., Alves, J., Mardones, D., et al. 2016, *A&A*, 587, A153
- Neupert, W. M. 1968, *ApJL*, 153, L59
- Osten, R. A., & Wolk, S. J. 2009, *ApJ*, 691, 1128
- Rau, U. 2012, in *Proc. SPIE*, Vol. 8500, *Image Reconstruction from Incomplete Data VII*, 85000N
- Rivilla, V. M., Chandler, C. J., Sanz-Forcada, J., et al. 2015, *ApJ*, 808, 146
- Rots, A. H. 2006, in *Astronomical Society of the Pacific Conference Series*, Vol. 351, *Astronomical Data Analysis Software and Systems XV*, ed. C. Gabriel, C. Arviset, D. Ponz, & S. Enrique, 73
- Salter, D. M., Hogerheijde, M. R., & Blake, G. A. 2008, *A&A*, 492, L21
- Sheehan, P. D., Eisner, J. A., Mann, R. K., & Williams, J. P. 2016, *ArXiv e-prints*, arXiv:1609.00025
- Wolk, S. J., Harnden, Jr., F. R., Flaccomio, E., et al. 2005, *ApJS*, 160, 423
- Zapata, L. A., Rodríguez, L. F., Kurtz, S. E., & O'Dell, C. R. 2004, *AJ*, 127, 2252

**Table 2.** Extreme radio variability in the ONC and X-ray properties

Src <sup>a</sup>	COUP	prev. ID <sup>b</sup>	<i>d</i>	$\Delta S_{\max}$ (0–2d)			$\Delta t_{\min}$ for x10 var.			$S_C$ <sup>c</sup>	CXO cnts <sup>d</sup>	varindex <sup>e</sup>	SpT <sup>f</sup>
		(radio)	(')	(ep.)	(30 min)	(6 min)	(ep.)	(30 min)	(6 min)	(mJy bm <sup>−1</sup> )	(0.5–8.0 keV)	(max)	
36	391	–	1.10	> 11	> 10	> 5	1d	27.0h	–	0.056±0.003	484.2	9	
53	427	–	2.40	13	> 12	> 7	1d	17.7h	–	0.165±0.004	514.4	9	
98	510	Zap 7, S	1.45	8	> 17	> 17	–	1.1h	0.7h	0.754±0.003	36.8	2	
110	530	GMR Q, S	0.51	6	11	> 6	–	24.9h	–	0.303±0.003	35.3	5	
189	640	S	0.76	10	34	> 25	1d	20.4h	19.3h	0.690±0.003	155.7	1	
254	745	GMR 12, KS	0.80	5	14	19	–	21.2h	20.5h	23.208±0.003	8048.8*	0	O9–B0.5
319	828	S	1.66	15	> 17	> 34	2d	41.1h	40.7h	2.358±0.003	5095.5*	0	K2–K6
414	985	K	2.21	8	9	> 13	–	–	22.9h	1.324±0.003	2391.7*	0	F8–K4
422	997	–	1.37	> 54	> 30	> 15	2d	41.1h	40.7h	0.676±0.003	2265.9*	6	K8
469	1101	S	1.79	2	12	> 14	–	1.1h	0.6h	0.235±0.003	3740.3*	10	M0+M3.5
489	1143	K	2.98	> 16	> 11	> 7	1d	27.6h	–	0.219±0.004	1430.8*	0	K1–K4
495	1155	–	1.91	5	> 10	> 7	–	47.4h	–	0.267±0.003	166.9	0	M3.5
515	1232	K	3.22	52	> 138	> 101	1d	0.5h	0.4h	1.188±0.004	7916.2*	10	O9.5–B2

<sup>a</sup> [FRM2016]<sup>b</sup> In (Zap) [Zapata et al. \(2004\)](#), (K) [Kounkel et al. \(2014\)](#) and (S) [Sheehan et al. \(2016\)](#).<sup>c</sup> Peak flux density, derived from the concatenated data in [Forbrich et al. \(2016\)](#).<sup>d</sup> Net counts, all four 2012 X-ray epochs combined; an asterisk denotes possible photon pile-up (see text).<sup>e</sup> Maximum varindex from the four CXO epochs (see text).<sup>f</sup> Spectral types as reported by [Hillenbrand et al. \(2013\)](#). Note that particularly in the case of the high-mass stars, the radio emission may be from unresolved lower-mass companions.